EUROPEAN ORGANIZATION FOR NUCLEAR RESEARCH

CERN-PPE/92-171
27 August 1992

KAPTON STRAW CHAMBERS FOR A TRACKING TRANSITION RADIATION DETECTOR

V. Bondarenko, B. Dolgoshein*), V. Grigoriev, O. Kondratiev, A. Medvedev, S. Pavlenko, M. Potekhin*,†), A. Romaniouk*), V. Sosnovtsev*), V. Tcherniatine*,‡)

Moscow Physical Engineering Institute

S. Muraviev*)

Lebedev Institute, Moscow

*) Visitor at CERN, Geneva, Switzerland.
†) Now at Columbia University, New York, NY, USA.
‡) Now at Brookhaven National Laboratory, Upton, NY, USA.

1 Introduction

Straw chambers have recenly become one of the popular devices in particle physics [1-7]. They have some virtues which make them useful for a variety of experiments, for example:

- Feasibility of high precision coordinate measurements at a gas pressure of up to 10 atm
- Isolation of a broken wire from its neighbours
- Self-supporting multistraw structure possibility
- Minimum cross-talk between neighbouring detector elements

Straw chambers are considered as a candidate tracking device in future collider experiments (SSC, LHC), which implies some specific requirements such as high radiation hardness and long-term durability of the conductive layer. Certain applications, like tracking Transition Radiation Detectors (TRDs) that are being developed by our group, necessitate high X-ray transparency of the straw chamber material [8,9]. Straw chambers are usually produced from mylar and/or polycarbonate films (see, for example, [3] and [5]). However, in view of the above requirements, a new solution for the straw material would be preferable.

Polyimide is one of the most radiation-hard polymers. It is X-ray transparent and has very good mechanical properties. We have developed a new technique for straw manufacturing, based on films of this plastic (kapton). As will be discussed below, straw chambers thus manufactured have a number of advantages.

We have investigated the properties of such chambers and present the results in the following sections:

- properties of the material and the straw production technology
- mechanical properties of the straw body
- electrical properties of the manufactured straw chambers
- the straw chamber performance and energy resolution
- spatial resolution
- radiation hardness of the kapton straw.

2 Properties of the material and the straw production technology

The kapton film used for the fabrication of straw is composed of four layers:

- a 18 μm base kapton film, providing mechanical strength
- on one side – 3 μm welding layer based on polyurethane composite
- the other side of the base film has high conductivity coating - 2000 Å of aluminum
- the aluminium coating is protected from accidental electric discharge and etching by a 4 μm layer with the bulk conductivity (polyimide + carbon powder).

The bulk conductivity layer has yet another function: the work function of carbon (4.7 eV) is higher than that of aluminum (4.3 eV), so a carbon cathode is less prone to photoeffect than an aluminum one. The kapton film manufactured by the above technology has surface conductivity of about 5 Ω/cm^2. Figure 1 shows the measured resistivity of a sample film strip (1×10 cm) as a function of elongation of the strip under the influence of an external force. There is a steep rise in the film resistivity after 2% elongation. Apparently

it is caused by destruction of the aluminium layer. This elongation corresponds to the beginning of nonlinear film deformation.

The straw tubes are prepared by spiralling on a mandrel of kapton film tapes (5 mm wide) at a temperature of about 200 °C. This continuous process provides straws of up to 5 m length. The total resulting thickness of the straw wall is about 50 μm.

The X-ray transparency of the straw wall was checked with 5.9 keV photons. It has been measured to be better by approximately 35% than mylar of the same thickness in g/cm^2. Practically it means that a 50 μm wall of the kapton straw is equivalent to 30 μm mylar in terms of X-ray absorption.

3 Mechanical properties of the straw body

Mechanical properties of the straw body are very important in the detector design, so a number of relevant tests were performed.

First, for a straw to be operational, it has to be straight. We considered three ways to achieve this:

1. putting the straws in straight channels, prepared with adequate precision (for example in the foam radiator of a TRD [8-10]). The uniformity of the gas gain in a system of straw chambers assembled in such a way is about 1%. This corresponds to overall deviations of the anode wire from its ideal position of about 100 μm (fig. 2).
2. glueing the straws together, using a precisely machined surface as a reference. The accuracy one may obtain with this method is better than 100 μm [2,5,6,7].
3. stretching of straws [3, 9].

The latter way of getting the straws straight was specifically studied. Sample kapton straws (4 mm diameter, wall thickness 50 μm) were stretched and various parameters, changing in time, were measured. Non-elastic deformation was measured (a) at fixed elongation, and (b) at fixed force applied along the straw axis. Time dependence of the tension at fixed elongation (corresponding to 200 g primary tension) is shown in fig. 3. The stabilization of straw parameters occurs in approximately 2 hours. It follows by 30% tension fouling drop.

Non-elastic deformation at fixed tension was also checked. The 50 cm straw tube was stretched by 200 g weight, and absolute elongation as a function of time was recorded. After a period of non-elastic deformation (2-3 hours) the length stabilizes. It remains the same within 10 μm accuracy at least for several months.

Figure 4 shows the straw deformation in a wide tension range. Essential deviation from linearity begins at a tension of more than 1500 g. The tension at which the straw destruction occurs is more than 3.5 kg. Absolute elongation of a 50 cm long straw is given in fig. 5. It corresponds to 300 μm per 100g of tension.

Typically, the straw has some curvature after manufacturing. To straighten it so that the gas gain is uniform at the level of $\pm$2% a force of more than 200 g should be applied (fig. 6). This corresponds to the anode wire eccentricity of $\sim$200 μm (fig. 2).

Measurements of the gas gain variation versus transversal force applied to the centre of the straw tube of 50 cm were done (fig. 7). The straw was stretched (the tension was 200 g) and its ends were fixed. A transversal force as small as 0.3 g leads to the gas gain change of more than 15%.

Figure 2(a) demonstrates the correlation between the anode wire eccentricity and the energy resolution when the chamber was irradiated with 5.9 keV quanta. Figure 2(b) shows the corresponding dependence of the gas gain in a certain point of the anode. A

gas mixture of 50% Xe and 50% CO_2 was used, at a gas gain of 5×10^3.

4 Electrical properties of the manufactured straw chambers

One of the conductive layers of our straw tube is a thin aluminium coating. It is deposited on the film by evaporation and has a surface resistivity of typically less than 1 Ω/cm^2. After deposition of the protective carbon composite (see sec.2) the resistivity of the conductive layer as a whole is 3–5 Ω/cm^2, so that typical resistance of a straw 50 cm long is about 400 Ω.

In case of low cathode resistance the characteristic impedance of the straw is given by $Z = \sqrt{L/C} \simeq 260\ \Omega$, frequency-independent. Unfortunately, the sum of the anode and cathode resistances cannot be neglected and the characteristic impedance becomes frequency dependent. Therefore, it is rather difficult to provide a good termination at the ends of the straw for the signals being read out, which have broad bandwidth. We have studied the termination problem, trying to minimize reflection of the real proportional-mode signal at the preamplifier end of the straw by varying the input impedance of the preamplifier. The best match was achieved at $Z = 300 - 330\Omega$ for the 5–10 ns rise time signal.

The attenuation length of the straw tube, considered as a transmission line for the fast proportional-mode signal is about 200 cm for the cathode straw resistivity of 8 Ω/cm.

It is worth pointing out that the straw resistance of 400–1000 Ω effectively helps equalize amplitudes of the signals originating in different points along the anode. For example, if the 50 cm straw had zero resistance, the amplitude difference between singnals from different ends of the chamber would have been $\sim$ 15–20%, with shaping time of electronics, say, 5 ns (due to reflection from an unterminated end). In the realistic case of 400–1000 Ω, however, this difference is less then 5%.

5 The straw chamber performance and energy resolution

Proportional mode characteristics of the straw were measured with different diameters of the anode wire – 20, 30 and 50 μm. Figure 8 shows the gas gain dependence on cathode voltage for gas mixtures based on Ar and Xe. The space-charge effects are clearly present. We have studied the space-charge effects in a 70% Xe + 20% CF_4 + 10% CO_2 mixture which, as a result of our previous research, was chosen for the straw chambers of the TRD. X-ray line sources of 1.65, 3.45, 5.9, 8.2 and 14.2 keV were used for this purpose. The most probable energy loss of β-particles from the ^{90}Sr source, corresponding in our case to 0.6 keV, was taken as a reference point: it was checked that there was no significant space-charge effect at this energy at gas gain values up to 3×10^4. The space-charge effect (percentage of the charge detected as a function of gas gain) is shown in fig. 9. At the gas gain of 2×10^4 only 70% of the charge deposited by a 5.9 keV X-ray is detected. The calibration curve for the gas gain 2×10^4 is given in fig. 10.

Typical amplitude resolution with Ar-and Xe-based gas mixtures is about 20% (FWHM) at 5.9 keV, with a variety of admixtures: CO_2, C_4H_{10} and CH_4. A mixture of Xe and CO_2 was shown to provide high drift velocity ($\simeq$50 μm/ns) [11]. A serious problem with this kind of mixtures is an occasional spark discharge between anode and cathode at high gas gains. To prevent this from happening, we add another component, CF_4, which also increases the electron drift velocity (fig. 11). The total drift time and energy resolution with such a mixture are shown in fig. 12 (conditions: 5.9 keV photons,

4 mm cathode diameter, 50 μm anode diameter).

As can be seen from fig. 12, the energy resolution in CF_4-containing mixtures is somewhat worse (due to electron attachment [11]). With this quencher the sparks are totally eliminated, instead, at high gas gains, self-quenching streamer(SQS) discharges occur [12], which do not have adverse effect on straws and do not lead to the amplifier breakdown. The SQS relative rate vs gas gain for Ar- and Xe-containing mixtures and for different anode diameters (20 μm, 50 μm) is shown in fig. 13. As can be seen in this figure, decreasing the anode wire diameter shifts the beginning of the SQS mode to a higher gas gain domain. It is our conclusion that triple mixtures like Xe + CO_2 + CF_4 are the best in terms of providing stability of the proportional mode and protection against sparks. SQS in these mixtures becomes significant at gas gains of 2×10^4.

It was shown in [11] that the total drift time depends on the anode wire diameter. We find that 50 μm is close to optimum from the point of view of minimizing the charge collection time and providing the appropriate range of stable straw operation.

6 Spatial resolution

The best coordinate resolution in case of the drift-time measurement is achieved with high gas gain, high pressure, fast electronics and low discriminator thresholds. However, in our case the gas gain is limited to $\simeq1.5\times10^4$ because the space-charge effect and SQS become significant at higher gas gains.

We have tested the coordinate measuring properties of the straw filled with the mixture of 70% Xe + 20% CF_4 + 10% CO_2. A simple set-up was used for this test (fig. 14). It had two straw chambers placed one behind another in a beam of 500 MeV electrons. The time difference between signals from the two straws was measured. The variance of this difference was used to estimate the timing, and, hence, coordinate, resolution (using the drift velocity curves shown in fig. 11). It is shown in fig. 15, for different thresholds. The best achieved resolution in this two-chamber set-up was 120 μm. We estimate that contribution of such factors as mechanical tolerances, multiple scattering and the beam particles, angular distribution to the resolution thus measured was not more than 25 μm. So most probably the 120 μm accuracy is determined by processes in the straw chamber itself: ionization statistics, ionization cluster size, timing uncertainty due to relatively slow signal ($\sim$ 8 ns rise time with 5.8 keV quanta), diffusion etc. Besides, there is another factor which can contribute — electron attachment to CF_4 molecules ([7,13,14]).

7 Radiation hardness of the kapton straw

Some results of our study of the radiation hardness of the kapton straw have been published [15]. Here we present the results obtained recently.

Several fully assembled straws of two kinds — of kapton and of polycarbonate [5] — were installed in a channel of a research nuclear reactor. The neutron spectrum peaked at 2.5 MeV, which is reasonably close to values expected in LHC experiments. The associated γ-radiation spectrum peaked at 0.6 MeV. The straws were exposed to a γ-ray dose of 80 Mrad, fast neutron fluence of 4×10^{14} cm^{-2} and slow neutron fluence of 1.7×10^{15} cm^{-2}, which is equivalent to more than 20 years of operation at highest projected LHC luminosity.

After being irradiated, the polycarbonate straws were found to be not gas-tight and hardly operational. The kapton straws, however, were still operational except for

one thing: the Cyanolit^{TM} glue used to fix the end plugs had been almost completely destroyed.

To supplement our study in [15], we also investigated the gas-dependent ageing effects in the straw chambers (20 cm long) filled with a mixture 70% Xe + 20% CF_4 + 10% CO_2, irradiated with a pulsed X-ray source. The typical gas gain was 10^4, gas flow 0.05 cm^3/min. The radiation dose was monitored by measuring the average straw current. The gas gain was measured at two different points along the straw: at the point where the straw was irradiated by X-rays and at the reference point, not exposed to radiation. The dependence of the ^{55}Fe peak amplitude on the total charge collected on the anode was looked at. No appreciable ageing effects were observed up to a cumulative charge of 5 C/cm, corresponding to approximately five years of highest luminosity operation at LHC.

Another important problem with radiation hardness of the straw chambers is the well-known cathode etching phenomenon, for instance, it was found in [16] that an aluminized mylar straw failed at a cumulative charge of 0.25 C/cm due to the destruction of the aluminum coating on the cathode. To avoid this, a 'thick' aluminium cathode (10 μm, [6]) or an aluminized polycarbonate [5] may be used. The thick aluminium cathode is not the best solution in terms of the amount of the material in the detector.

We have specifically tested our kapton straw and an aluminized polycarbonate straw to compare the etching phenomena in these two cases. Resistance of the 20-cm long straws was measured while they were irradiated (actually a spot with typical dimension of 3 cm along the anode was exposed to X-rays). The resistance of the kapton and aluminized polycarbonate straws as a function of total accumulated charge is given in fig. 16. Fast deterioration of the Al layer in the polycarbonate straw begins at $\sim$0.2 C/cm, followed by practically total evaporation of aluminium at $\sim$1 C/cm. At the same time, the kapton straw showed only a slight increase of the resistivity from 161.7 Ω to 164.2 Ω for the total accumulated charge of 2.6 C/cm. This, of course, is due to the protective carbon composite layer covering the vulnerable aluminium surface in the latter case.

8 Conclusions

We have tested the straw chambers of a new type, made of kapton film, with special focus on properties relevant for operation in the LHC environment. It has been demonstrated that stretching of the straws with a force the $\simeq$200 g guarantees uniformity of the gas gain at the level of $\pm$2%. Gas mixtures for this type of chamber were studied, and it was found that, for the TRD/tracker application, the desired stability and speed of operation can be achieved with 70% Xe + 20% CF_4 + 10% CO_2. Space-charge effects show up at gas gains of $\sim 10^4$. Spatial resolution, achieved with timing measurements, was estimated to be $\simeq$120 μm.

Exceptional radiation hardness of the kapton straw chambers, proved in our experiments, as well as the long lifetime of the electrodes, drive us to the conclusion that many-year operation of the chambers at maximum projected LHC luminosity is possible.

Acknowledgements

We wish to thank A. Konstantinov, S. Konovalov and V. Laktionov for their help. We are also grateful to S. Whittaker and J. Shank of Boston University, who provided us with the polycarbonate straw samples.

REFERENCES

[1] C. Broll et al., Nucl. Instr. and Meth. **206** (1983) 385.
[2] P.B. Baringer et al., Nucl. Instr. and Meth. **A254** (1987) 542.
[3] W.T. Ford et al., Nucl. Instr. and Meth. **A255** (1987) 486.
[4] S. Bhara et al., Nucl. Instr. and Meth. **A268** (1988) 92.
[5] M. Frautschi et al., Nucl. Instr. and Meth. **A307** (1991) 52.
[6] C. Bromberg et al., Nucl. Instr. and Meth. **A307** (1991) 292.
[7] S.H. Oh et al., Nucl. Instr. and Meth. **A309** (1991) 368.
[8] V.A. Polychronakos et al., CERN/DRDC/90-38 (1990).
[9] J.T. Shank et al., Nucl. Instr. and Meth. **A309** (1991) 337.
[10] V.A. Polychronakos et al., CERN/DRDC/91-47 (1991).
[11] B. Dolgoshein et al., Nucl. Instr. and Meth. **A294** (1990) 473.
[12] G. D.Alekseev et al., Nucl. Instr. and Meth. **153** (1978) 157.
[13] S. F.Biadi, Nucl. Instr. and Meth. **A310** (1991) 133.
[14] C. Neyman et al., SDC notes, SDC-90-00054 (1990).
[15] V. Bondarenko et al., CERN-PPE/91-191 (1991).
[16] H. N.Nelson, SLAC-PUB-4318 (1987).

Figure captions

Fig. 1. The dependence of the energy resolution (a) and the gas gain (b) with 5.9 keV photons on eccentricity of the anode wire
Fig. 2. Resistance of the kapton film vs its elongation
Fig. 3. Straw tension variation in time, at fixed straw length
Fig. 4. The straw deformation curve
Fig. 5. Absolute elongation of a 50-cm long straw vs tension
Fig. 6. Gas gain variation along the sample straw
Fig. 7. Gas gain variation vs transversal force applied in the middle of the straw. Straw length 50 cm, straw tension 200 g
Fig. 8. Gas gain as a function of HV in straws filled with Xe- and Ar-based mixtures
Fig. 9. Space-charge effect (as a percentage of the charge observed) as a function of gas gain.
Fig. 10. Sample calibration curve for the gain of 2×10^4
Fig. 11. Drift velocity in Xe-based mixtures vs electric field
Fig. 12. Total drift time and energy resolution with 5.9 KeV photons as a function of CF_4 percentage in the mixture. Cathode diameter 4 mm, anode diameter 50 μm.
Fig. 13. Dependence of the relative weight of SQS mode on the gas gain, for Xe- and Ar-based mixtures
Fig. 14. Experimental set-up for the spatial resolution measurements: VETO, S_1, S_2 — scintillation counters; PA+SA — preamplifier and shaper with a rise-time of 8 ns; T-A — time-to-amplitude converter; T_1 and T_2 — times of arrival of the signals from the two straws respectively
Fig. 15. Spatial resolution of the straw chamber filled with 70% Xe + 20% CF_4 + 10% CO_2, as a function of the discriminator threshold
Fig. 16. Resistivity of the polycarbonate and kapton straws vs total accumulated charge

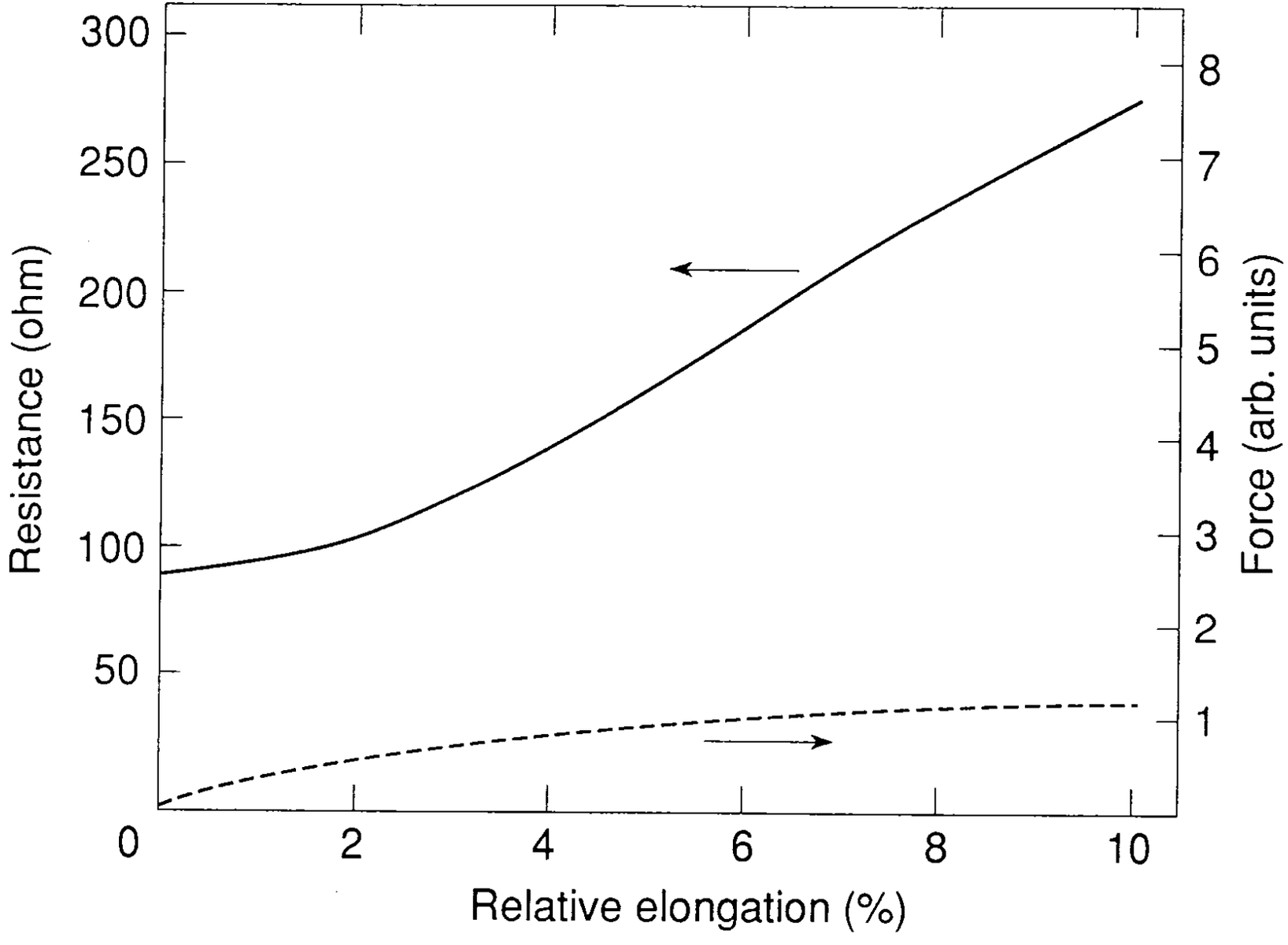
300
250
200
150
100
50
0
2
4
6
8
10
Resistance (ohm)
Force (arb. units)
8
7
6
5
4
3
2
1
Relative elongation (%)

Fig. 1

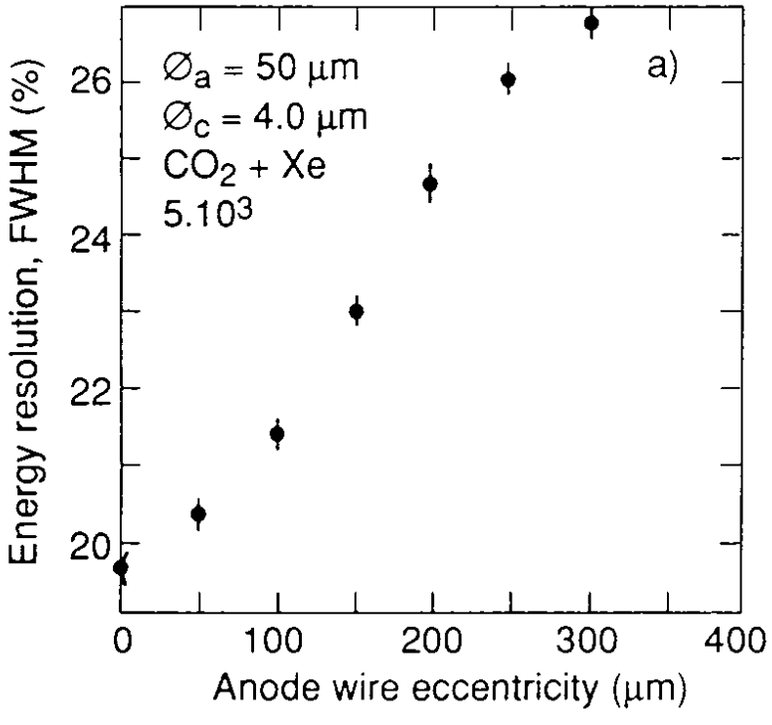
Energy resolution, FWHM (%)
26
24
22
20
$\varnothing_a$ = 50 µm
$\varnothing_c$ = 4.0 µm
CO_2 + Xe
5.10^3
a)
0
100
200
300
400
Anode wire eccentricity (µm)

(a)

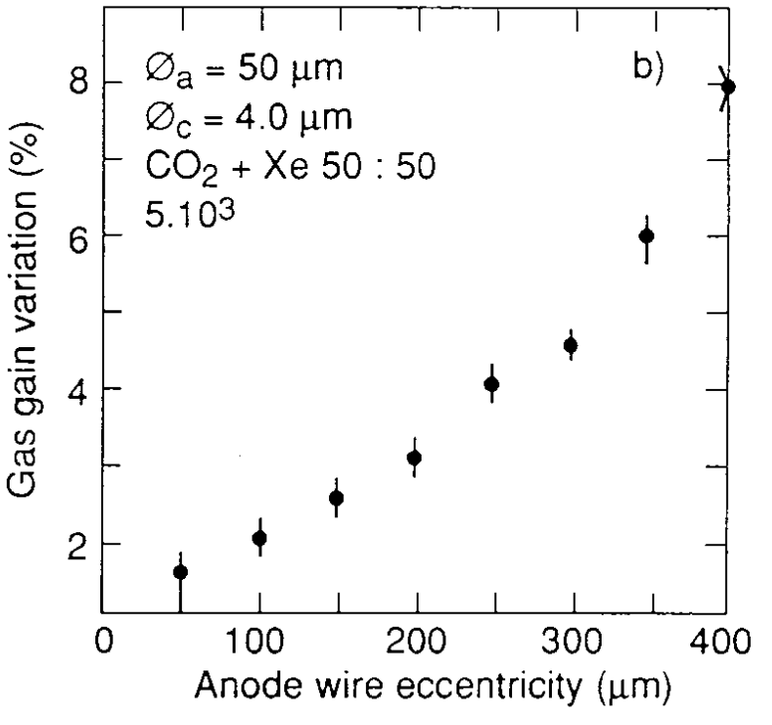
Gas gain variation (%)
8
6
4
2
$\varnothing_a$ = 50 µm
$\varnothing_c$ = 4.0 µm
CO_2 + Xe 50 : 50
5.10^3
b)
0
100
200
300
400
Anode wire eccentricity (µm)

(b)

Fig. 2

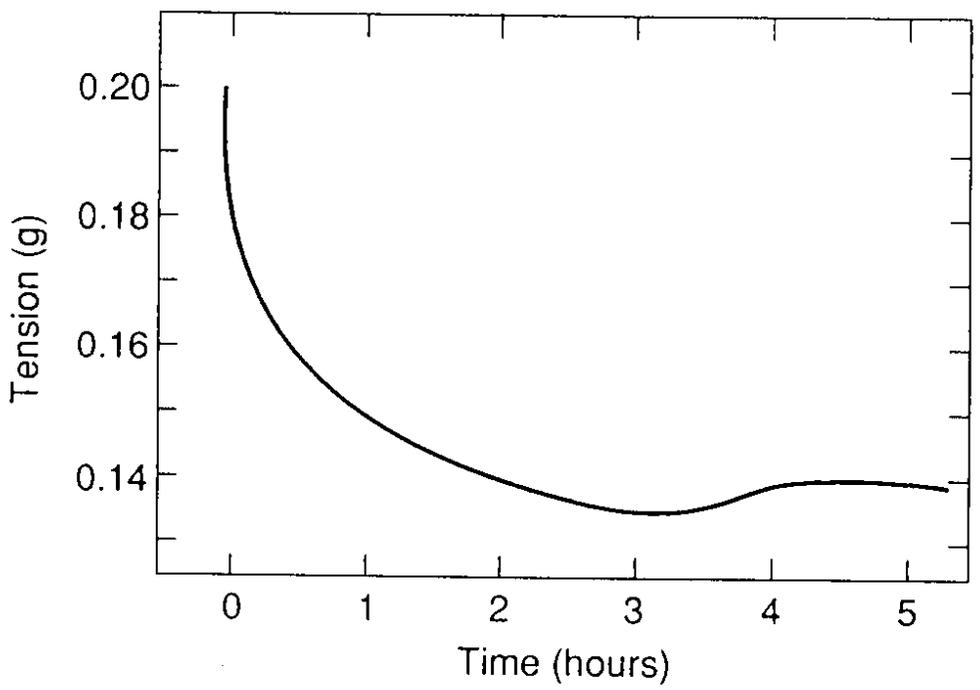

Fig. 3

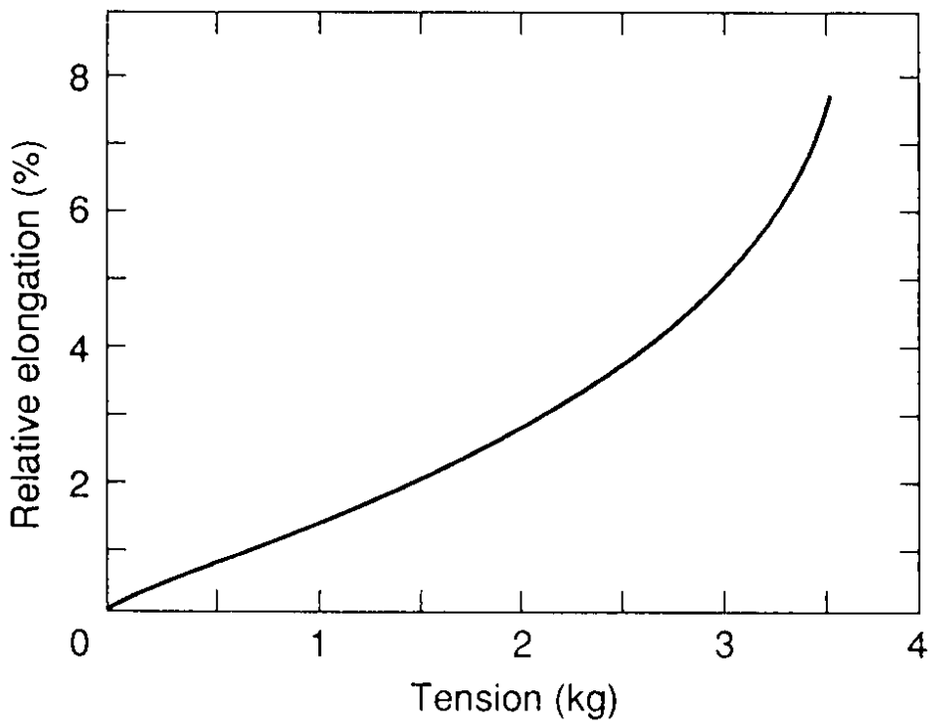

Fig. 4

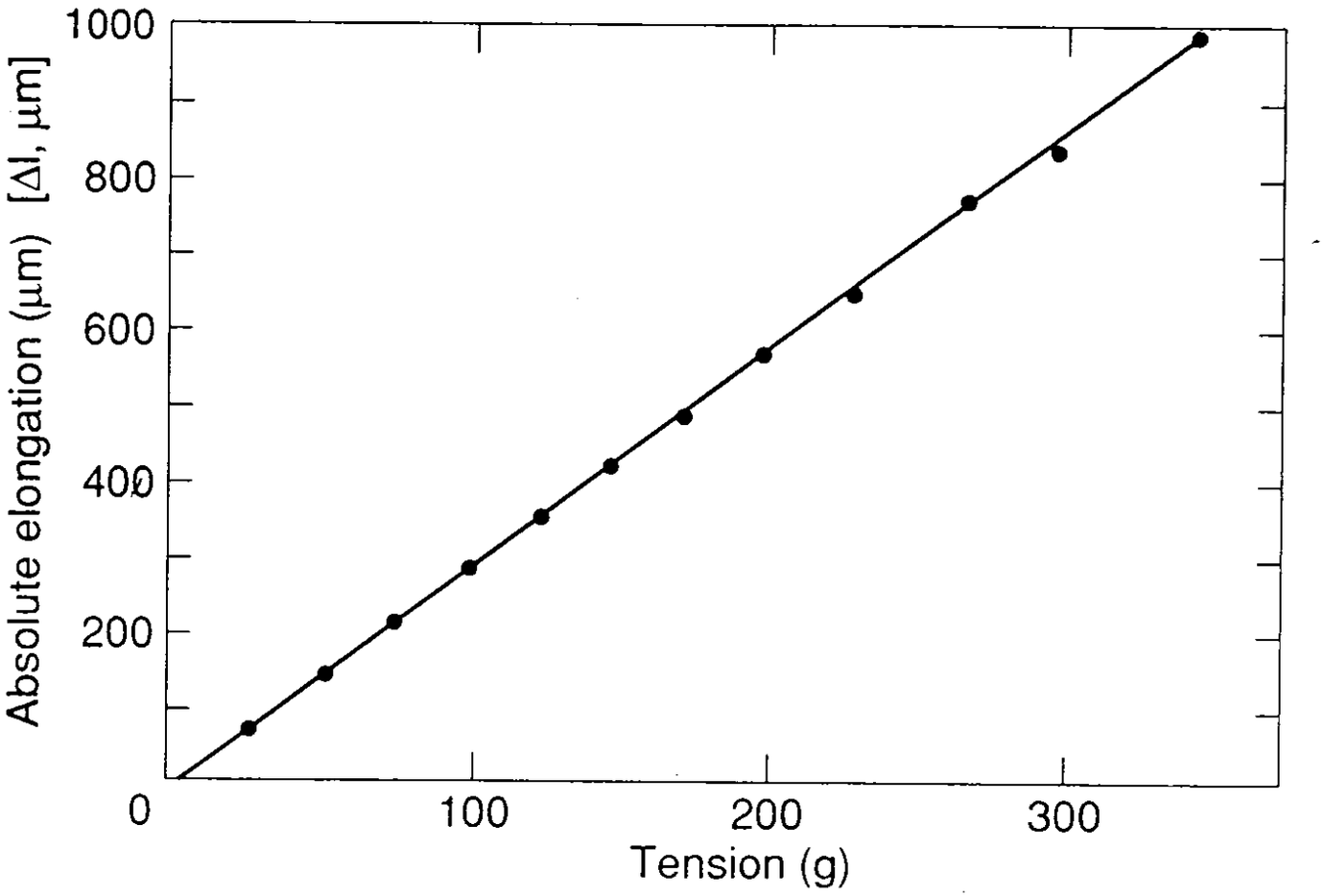
Absolute elongation (μm) [Δl, μm]
1000
800
600
400
200
0
100
200
300
Tension (g)

Fig. 5

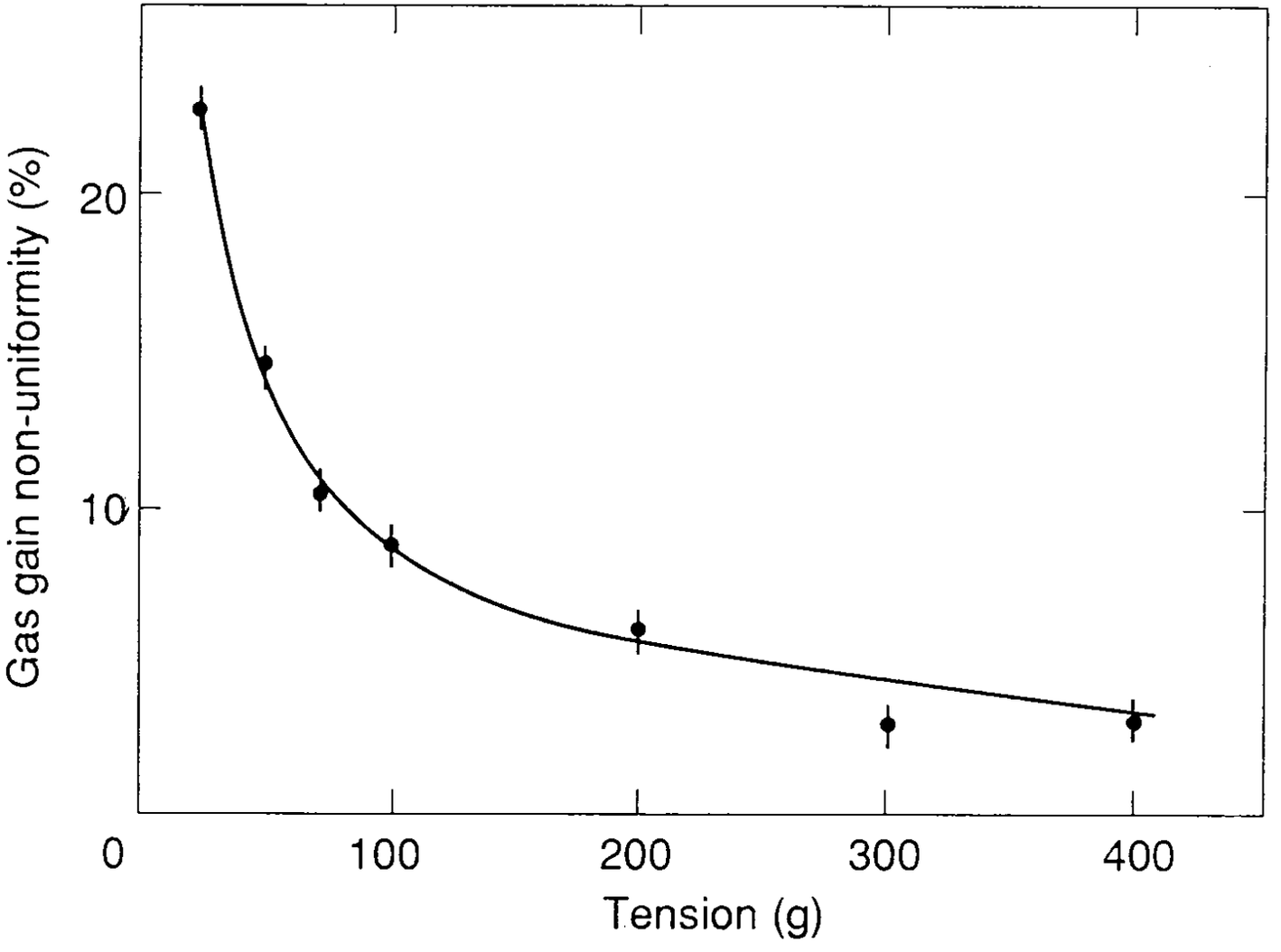

Fig. 6

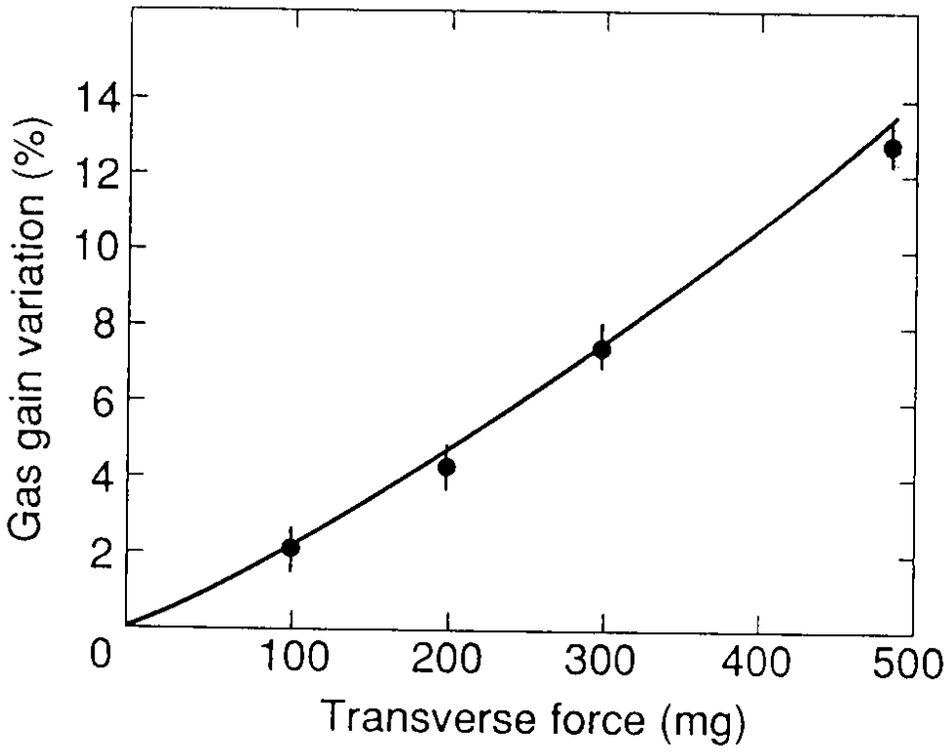
Gas gain variation (%)
0
2
4
6
8
10
12
14
100
200
300
400
500
Transverse force (mg)

Fig. 7

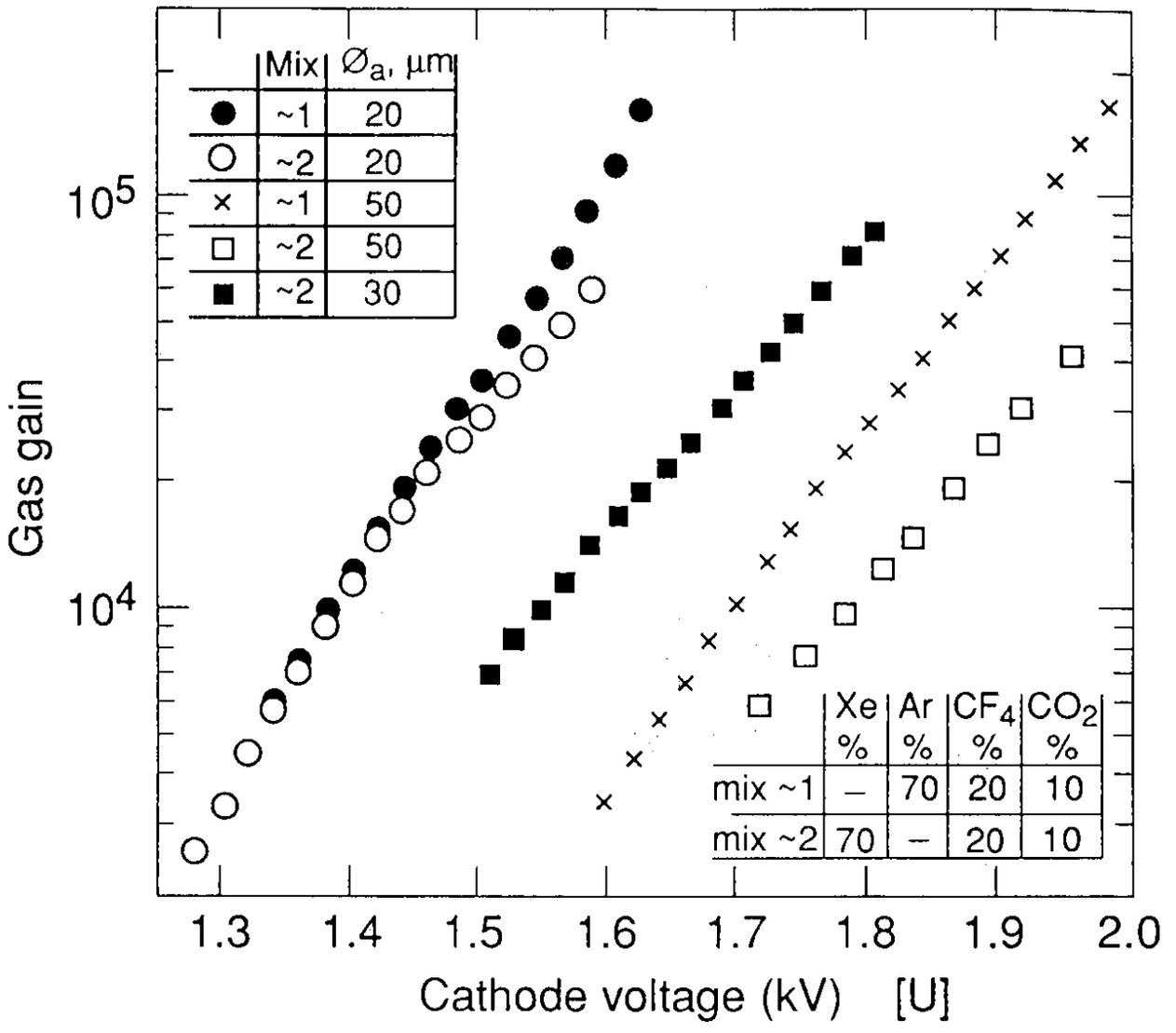
Mix
Ø_a, µm
~1 20
~2 20
~1 50
~2 50
~2 30
Gas gain
10^5
10^4
1.3
1.4
1.5
1.6
1.7
1.8
1.9
2.0
Cathode voltage (kV) [U]
Xe %
Ar %
CF4 %
CO2 %
mix ~1 – 70 20 10
mix ~2 70 – 20 10

Fig. 8

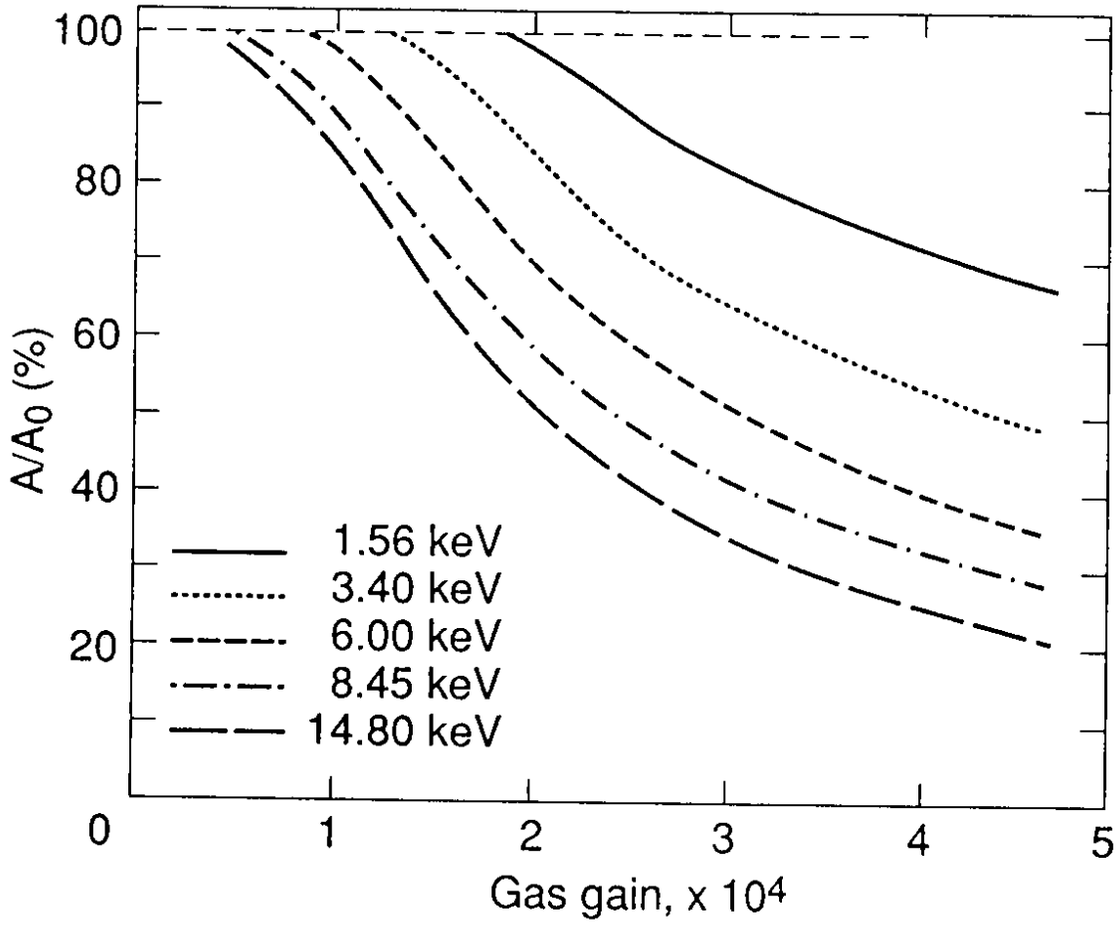
100
80
60
40
20
0
A/A0 (%)
1.56 keV
3.40 keV
6.00 keV
8.45 keV
14.80 keV
1
2
3
4
5
Gas gain, x 10^4

Fig. 9

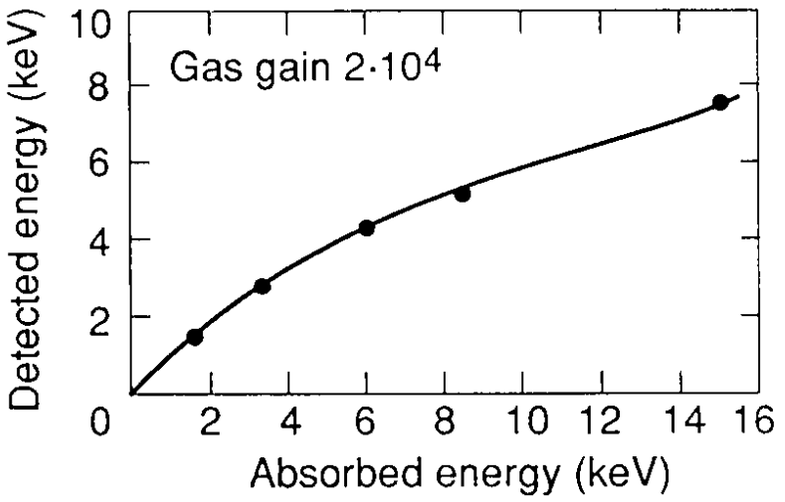
Gas gain 2·10⁴
Detected energy (keV)
Absorbed energy (keV)
0
2
4
6
8
10
12
14
16

Fig. 10

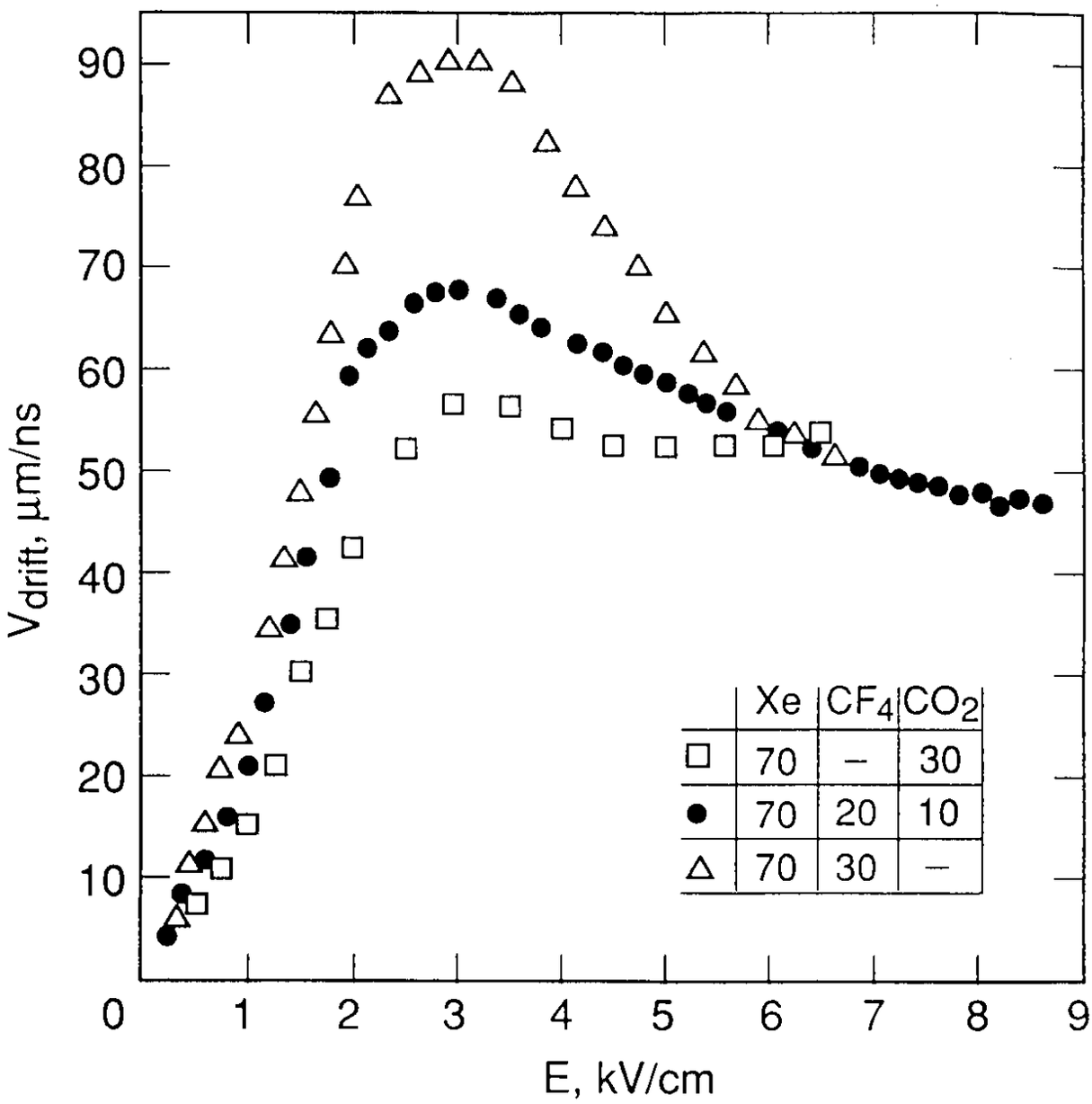
90
80
70
60
50
40
30
20
10
0
1
2
3
4
5
6
7
8
9
V_{drift}, μm/ns
E, kV/cm
Xe
CF_4
CO_2
70 – 30
70 20 10
70 30 –

Fig. 11

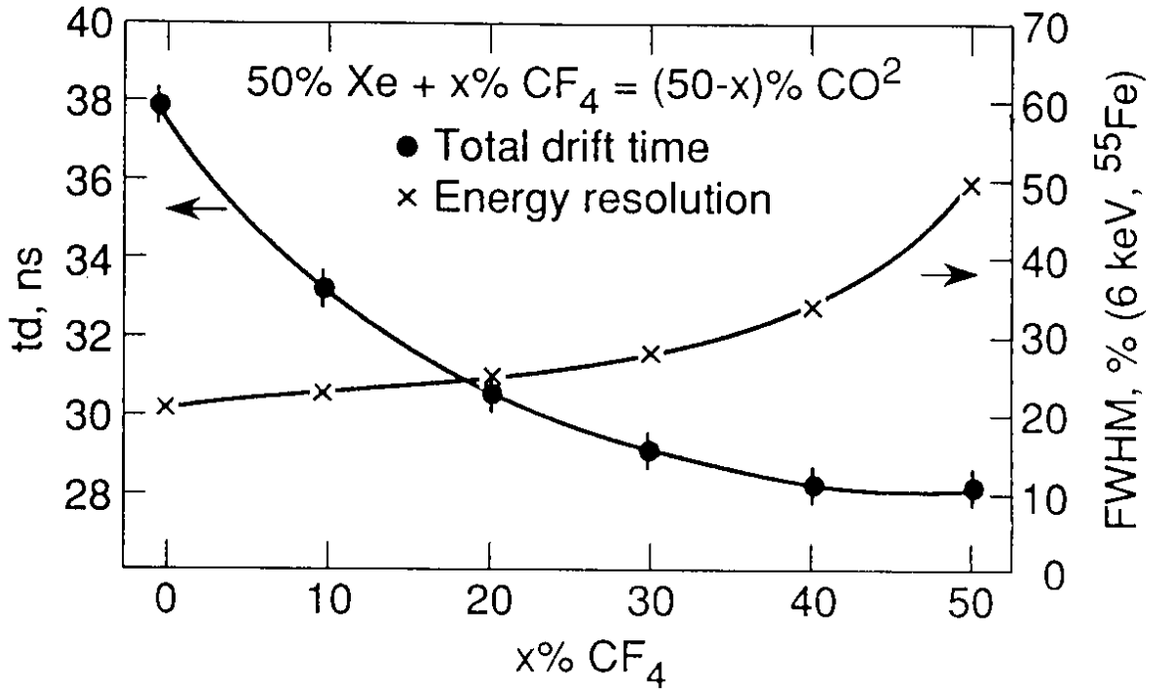
50% Xe + x% CF_4 = (50-x)% CO^2
● Total drift time
× Energy resolution
td, ns
FWHM, % (6 keV, ^{55}Fe)
x% CF_4
40
38
36
34
32
30
28
70
60
50
40
30
20
10
0
0
10
20
30
40
50

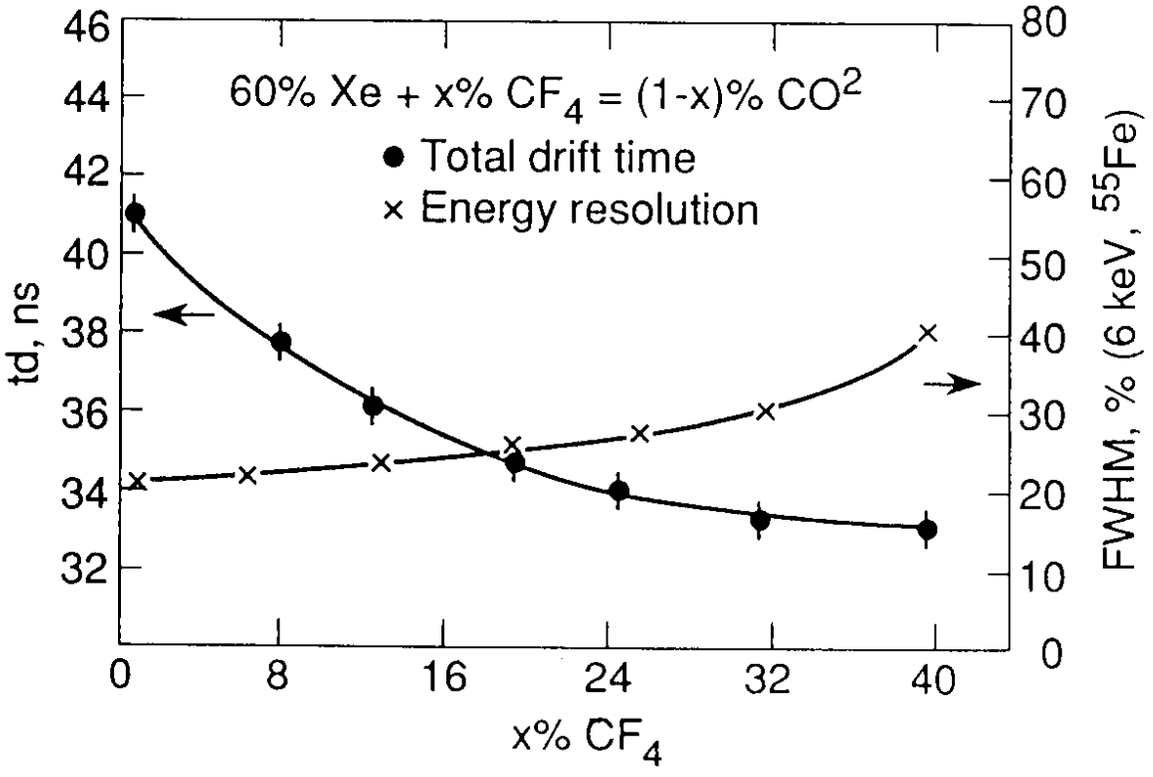
60% Xe + x% CF_4 = (1-x)% CO^2
● Total drift time
× Energy resolution
td, ns
FWHM, % (6 keV, ^{55}Fe)
x% CF_4
46
44
42
40
38
36
34
32
80
70
60
50
40
30
20
10
0
0
8
16
24
32
40

Fig. 12

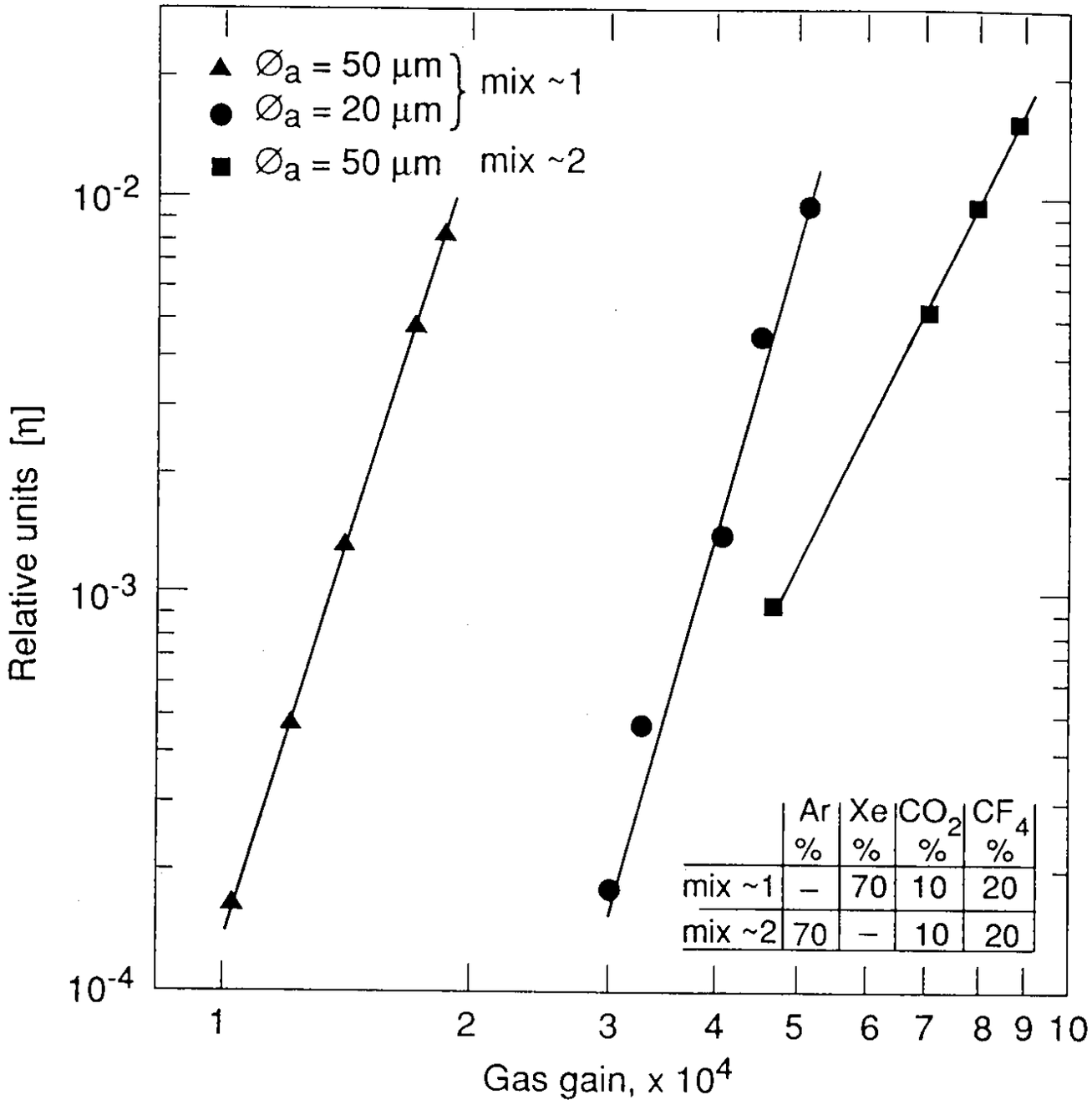
▲ ∅a = 50 μm
● ∅a = 20 μm
mix ~1
■ ∅a = 50 μm mix ~2
Relative units [η]
10-2
10-3
10-4
1
2
3
4
5
6
7
8
9
10
Gas gain, x 10^4
Ar % Xe % CO2 % CF4 %
mix ~1 – 70 10 20
mix ~2 70 – 10 20

Fig. 13

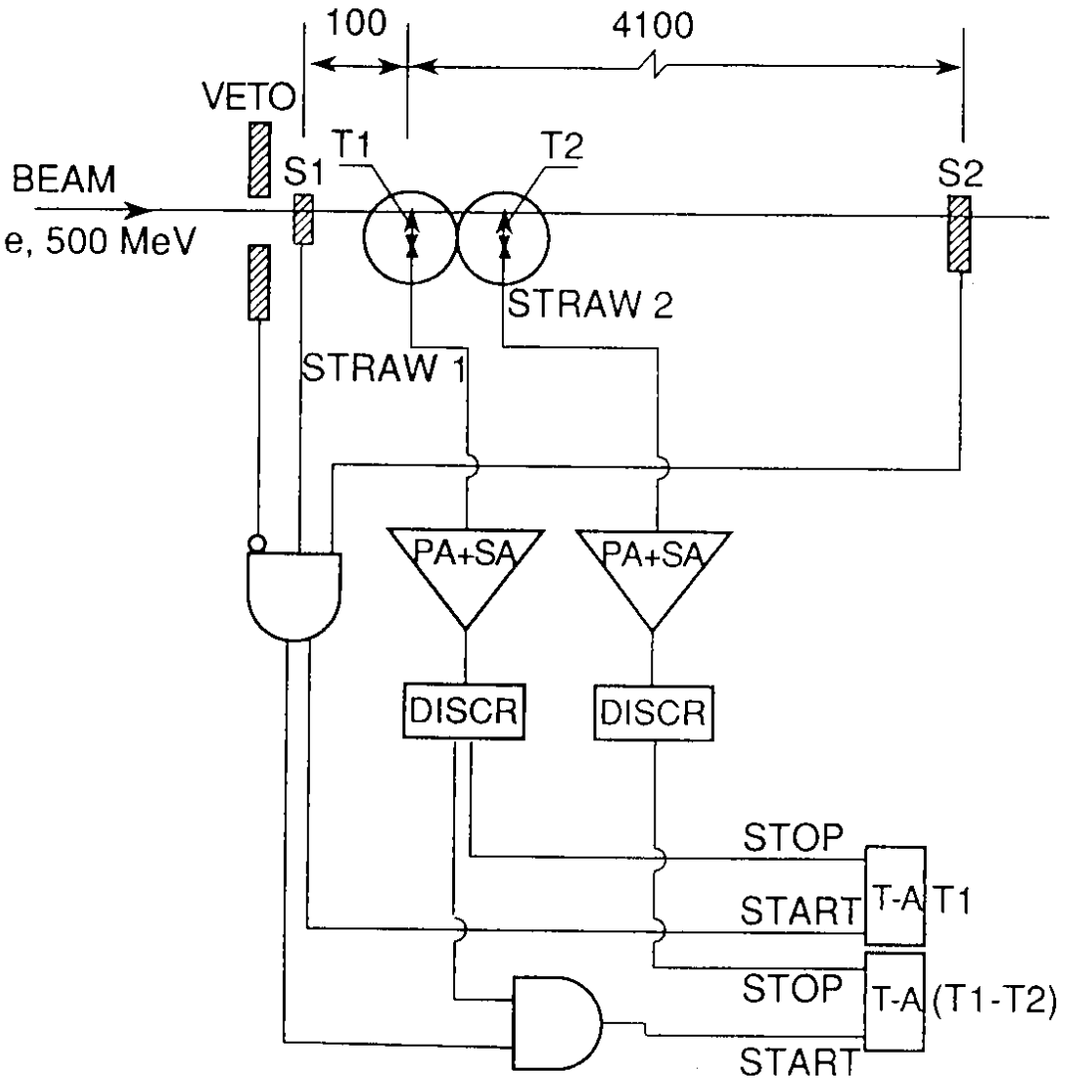
100
4100
VETO
T1
T2
BEAM
S1
S2
e, 500 MeV
STRAW 2
STRAW 1
PA+SA
PA+SA
DISCR
DISCR
STOP
START
T-A
T1
STOP
T-A
(T1-T2)
START

Fig. 14

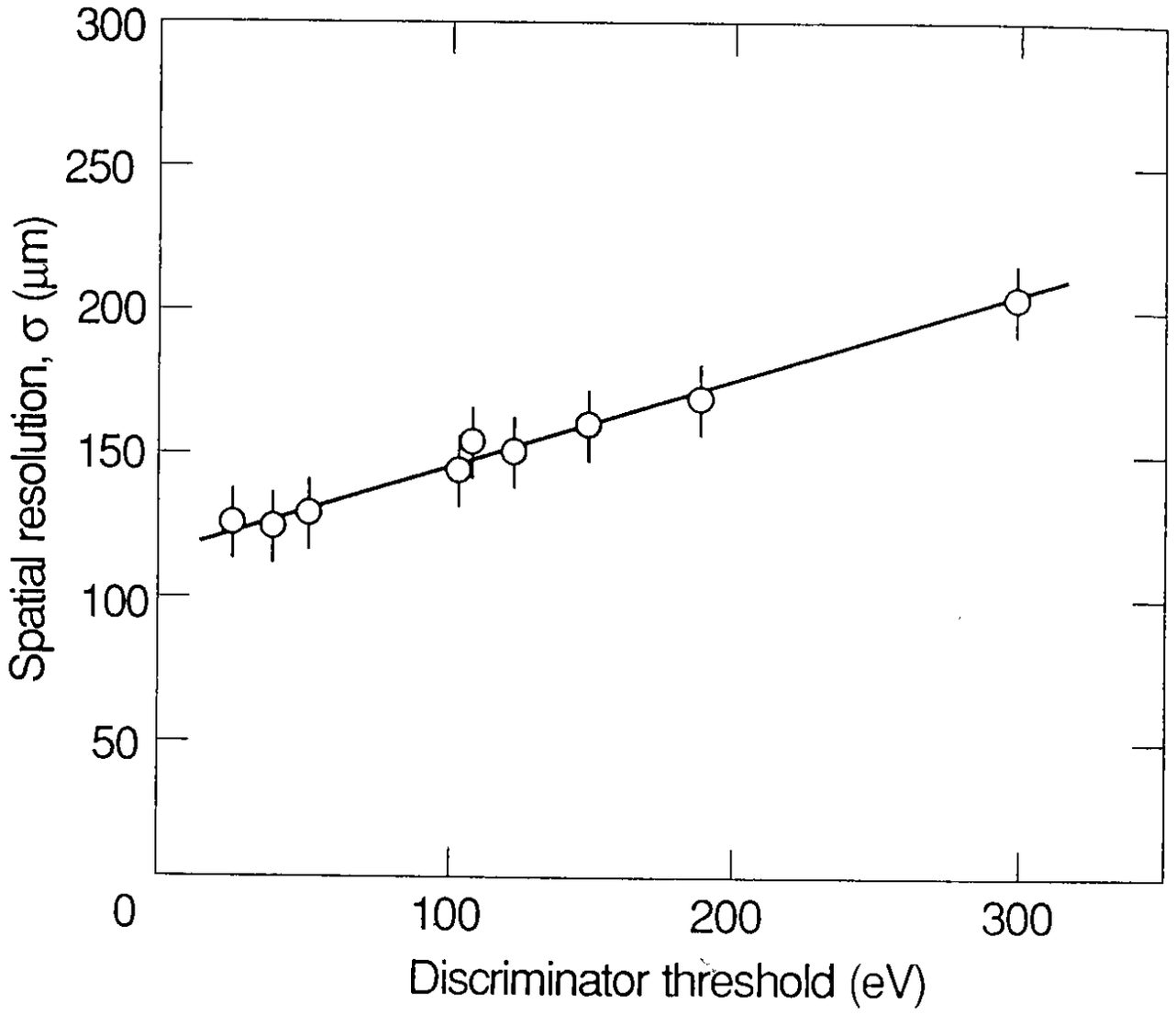
300
250
200
150
100
50
0
100
200
300
Spatial resolution, σ (μm)
Discriminator threshold (eV)

Fig. 15

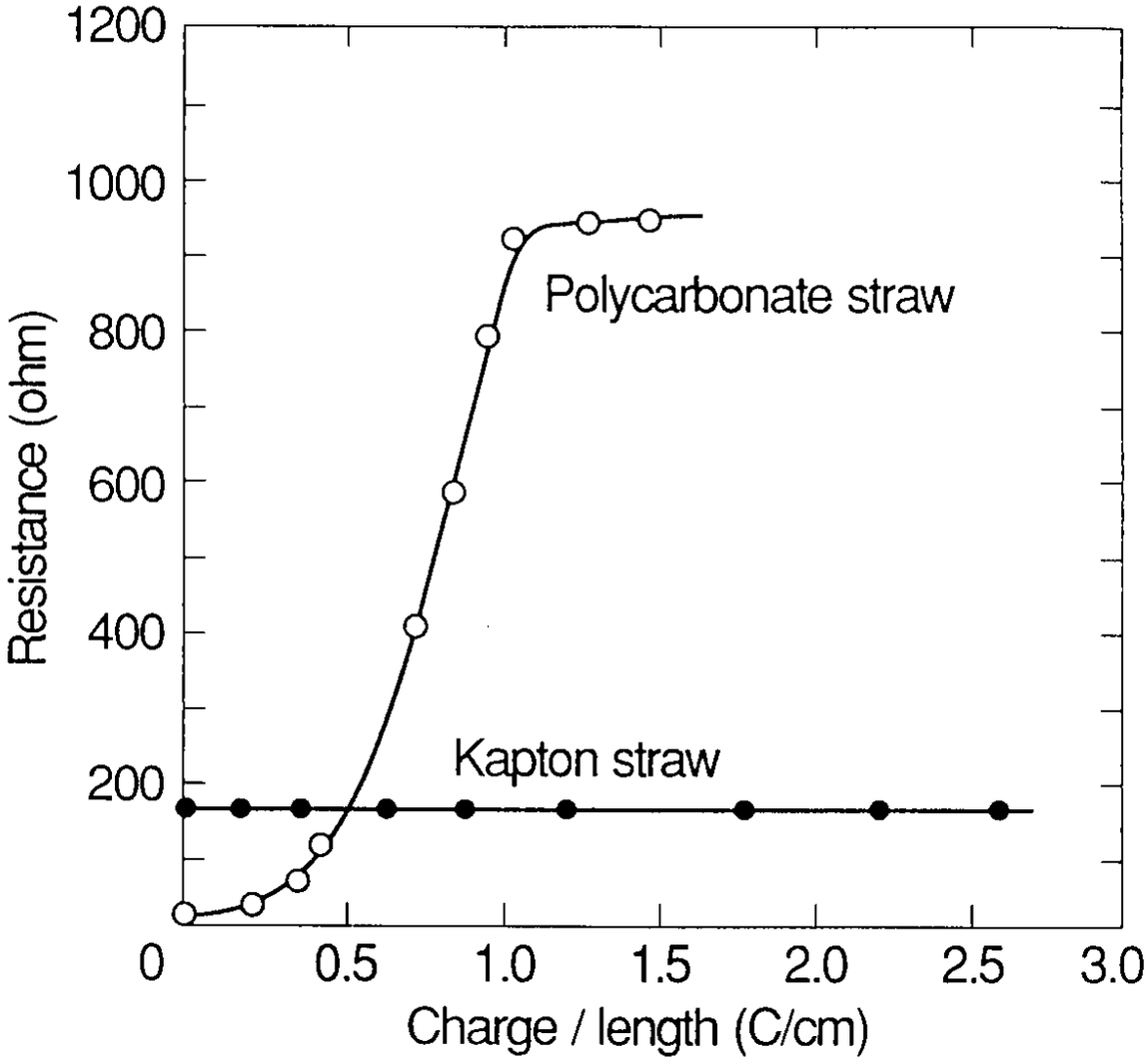
1200
1000
800
600
400
200
0
Resistance (ohm)
Polycarbonate straw
Kapton straw
0.5
1.0
1.5
2.0
2.5
3.0
Charge / length (C/cm)

Fig. 16